



PARAMETRIC INSTABILITY OF A BEAM UNDER ELECTROMAGNETIC EXCITATION

C.-C. CHEN

*Department of Mechanical Engineering, Dahan Institute of Technology, Hualien 971, Taiwan,
Republic of China*

AND

M.-K. YEH

*Department of Power Mechanical Engineering, National Tsing Hua University, Hsinchu 30043 Taiwan,
Republic of China. E-mail: mkyeh@pme.nthu.edu.tw*

(Received 3 April 2000, and in final form 10 August 2000)

The parametric instability of a beam under electromagnetic excitation was investigated experimentally and analytically. In experiment an electromagnetic device, acting like a spring with alternating stiffness, was designed to parametrically excite the beam. The frequency and the amplitude of the excitation force were accurately controlled by the AC current flowing through the coil of the electromagnetic device. Since the excitation force is a non-contact electromagnetic force which acts on the beam in the transverse direction, the disturbances induced by the geometric imperfection of the beam, by the eccentricity of the usual axial excitation force, and the coupling effects between the excitation mechanism and the beam were effectively avoided. The dynamic system was analyzed based on the assumed-modes method. The instability regions of the system were found to be the functions of the modal parameters of the beam and the position, the stiffness of the electromagnetic device for various cantilevered beams. The modal damping ratios of the beam specimens were also identified. The experimental results were found to agree well with the analytical ones.

© 2001 Academic Press

1. INTRODUCTION

The parametrically excited instability of structural elements has been studied considerably in recent years. Bolotin [1] summed up this problem of various structural elements in his book. Extensive bibliographies on this subject were also given by Evan-Iwanoski [2] and Nayfeh and Mook [3]. Essentially, the governing equation of parametric excitation problem can be expressed as the Mathieu–Hill equation. Some researchers [4–8] used analytical methods to solve the Mathieu–Hill equation with different conditions. Iwatsubo *et al.* [9, 10] used numeric simulation procedures to examine the instability regions of the Mathieu–Hill equation.

On the investigation of beams or columns, many studies focused analytically or numerically on the instability behavior of systems with various boundary conditions, various excitation methods, and various material properties. Iwatsubo *et al.* [9–11] examined numerically the parametric resonances of a beam with various boundary conditions under the excitation of a periodic axial or tangential loading at one end. Evensen and Evan-Iwanowski [12] investigated analytically the principal resonance of a simply

supported column subjected to a periodic axial loading at one end; they discussed the effects of longitudinal inertia upon the parametric response of the column. Sato *et al.* [13] studied the variation of the instability regions induced by the weight and position of a concentrated mass on a simply supported beam. Yeh and Chen [14] investigated analytically a general column under a periodic load in the direction of the tangency coefficient at any axial position; they gave the physical explanations of the parametric resonances by viewing the system energy. Handoo and Sundararajan [15] studied the principal instability regions of cantilevered columns having longitudinal inertia and end mass. Elmaraghy and Tabarrok [16] examined the dynamic resonances of a beam with clamped ends under an axial oscillation at one end. Saito and Koizumi [17] and Gürgöze [18] investigated the instability phenomena of a simply supported beam carrying a concentrated mass at one end and subjected to an axial oscillation at the other end. Buffinton and Kane [19] examined numerically the parametric instability of a beam that periodically oscillated between two fixed simply supported points. Gürgöze [20] investigated the dynamic instability of a pre-twisted beam subjected to a pulsating axial force for various types of boundary conditions. Chen and Yeh [21] assessed the simple and combination resonances of a general column carrying an axially oscillating mass. Stevens and Evan-Iwanowski [22] and Cederbaum and Mond [23] investigated the instability properties of viscoelastic columns under a periodic axial loading. Gürgöze [24] studied the parametric behavior of a viscoelastic beam subjected to a steady axial load and a transverse displacement excitation at one end. Ray and Kar [25, 26] examined numerically the parametric instability of multi-layered sandwich beams and partially covered sandwich beams under a periodic axial loading.

However, few studies have been made on the experimental observation of the instability behavior of beam or column systems. Bolotin [1] examined experimentally the principal instability region at twice the fundamental frequency of a simply supported column subjected to a periodically axial force at one end. Iwatsubo *et al.* [10] studied experimentally the simple and combination resonances of clamped-clamped and clamped simply supported columns under a periodic axial load. Evensen and Evan-Iwanowski [12] experimentally observed the principal simple resonance of an elastic simply supported column under a periodically axial end loading with the effects of longitudinal inertia. Handoo and Sundararajan [15] experimentally investigated the simple resonance of a cantilevered column with an end mass subjected to specified axial motion at its fixed end. Stevens and Evan-Iwanowski [22] observed the principal instability region of a viscoelastic simply supported column under a periodically axial force.

The experimental studies mentioned above focused on the systems subjected to a “periodically axial loading” or “periodically axial motion”. The instability regions of these problems are obviously disturbed by the initial curvature of the beam or column axis, the coupling effects between the excitation mechanism and the specimen, and the eccentricity of the longitudinal force [1].

In this work, a new electromagnetic device was developed in experiment to observe the instability phenomena of a beam under parametric excitation. The advantages of this device are: (1) the non-contacting electromagnetic excitation force; (2) the excitation force acting on the beam in the transverse direction; and (3) the accurately controlled frequency and amplitude of the excitation force by AC power source. Hence, the disturbances induced from the geometric imperfection of the beam, the eccentricity of the longitudinal force and the coupling effects between the excitation mechanism and the beam were effectively avoided. The experimental results are found to be in good agreement with the analytical results.

2. INSTABILITY EXPERIMENT

The instability experiment of a beam excited parametrically was performed using a self-designed electromagnetic device. The experiment was divided into two major phases: (1) to identify a relationship between the DC current through the coil and the stiffness of an electromagnetic device; and (2) to observe the instability behavior of a beam under parametric excitation caused by the electromagnetic device. This electromagnetic device, possessing time-varying stiffness, acts like an electromagnetic spring applied on the beam transversely. As shown in Figures 1 and 2, the electromagnetic device consisted of a pair of magnets and a pair of coils. The pair of magnets were fixed on support connected to the ground. An enameled wire was wound around a plastic frame to form the coils. The plastic frame was mounted on the beam and the reliable excitation frequency bandwidth of the electromagnetic device assured. As the current flows through the coil, the coil becomes an electromagnet. The mutual acting forces between the electromagnet and the pair of magnets make the electromagnetic device function like a spring. When the DC coil current has the same direction as shown in Figure 1, the mutual acting forces between the electromagnet and the pair of magnets are repulsive forces. The resultant force acting on the electromagnet by the pair of magnets tends to push the beam back to the undeformed central line from the deformed position. In this case, the electromagnetic device has positive stiffness. When the DC coil current has the opposite direction to that shown in Figure 1, the mutual acting forces between the electromagnet and the pair of magnets are attractive forces. The resultant force acting on the electromagnet by the pair of magnets tends to pull the beam away from the undeformed central line. The electromagnetic device acts like a spring with negative stiffness. Besides, when the coil current is an AC current, the electromagnetic device becomes a spring with alternating stiffness. The electromagnetic device was employed as a “non-connecting shaker” to induce parametric excitation on the beam.

2.1. IDENTIFYING SPRING STIFFNESS OF THE ELECTROMAGNETIC DEVICE

Figures 3 and 4 show, respectively, the schematic and the experimental set-up to measure the natural frequency of the beam specimen by applying a DC coil current. The cantilevered

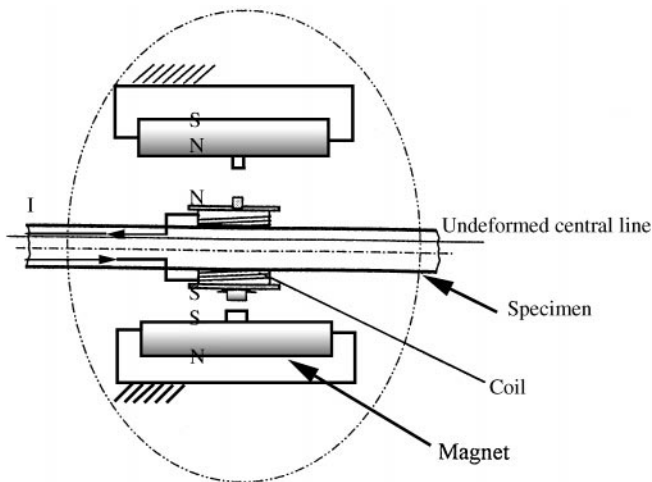


Figure 1. Schematic of the electromagnetic device.

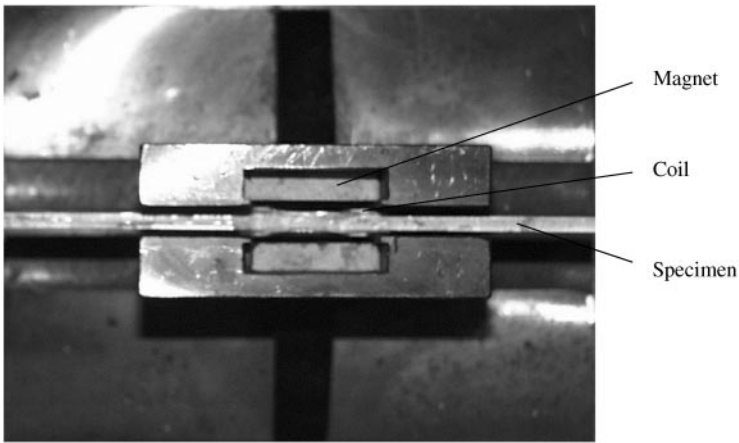


Figure 2. Electromagnetic device.

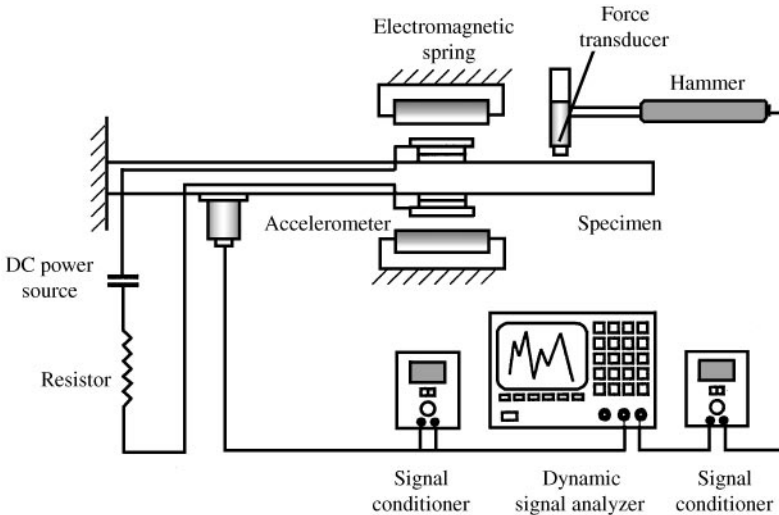


Figure 3. Schematic for measuring the natural frequency of specimens.

beam specimen was equipped with an electromagnetic device powered by a DC source to supply additional stiffness to the specimen. An impact hammer with a force transducer was used to excite the beam specimen. An accelerometer was used to measure the dynamic behavior of the specimen. Two signal conditioners were used to provide constant current power to the accelerometer and the force transducer, whose signals were analyzed and displayed on a dynamic signal analyzer.

Six cantilevered beam specimens, labelled from CF1 to CF6, were used in experiments. An electromagnetic device, equivalent to a concentrated mass and a variable stiffness spring at the connecting point, was mounted on each specimen. The detailed physical dimensions and properties of each specimen are given in Table 1. The experiments were conducted and repeated for each specimen at various DC coil currents. The relationship between the variation of the transverse fundamental frequency of each specimen and the DC coil

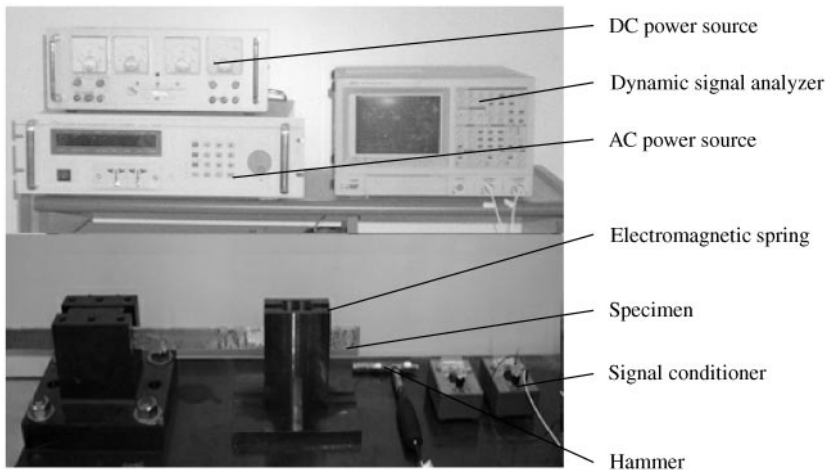


Figure 4. Experimental set-up for measuring the natural frequency of specimens.

currents was measured. Figure 5 shows the relationship between the fundamental frequency of the beam and the DC coil current of the electromagnetic device for specimen CF5. After comparing the experimental results with the analytical ones, the relationship between the stiffness of the electromagnetic device and the DC coil current was identified. It is noted that the excitation force was applied lightly enough to avoid the non-linear effects resulting from the deformation of the beam and the relative displacement between the electromagnet and the magnets.

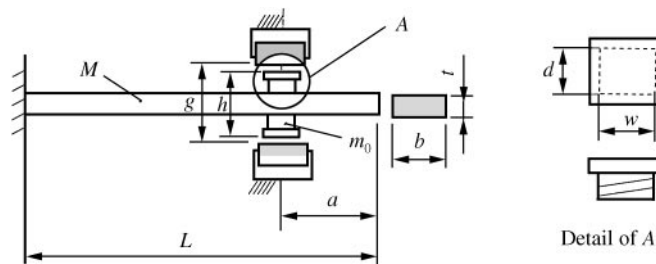
2.2. OBSERVING THE INSTABILITY BEHAVIOR OF SPECIMEN

Figure 6 shows the experimental set-up to observe the instability behavior of the beam specimen excited by an electromagnetic device. The electromagnetic device was powered with an AC source. The dynamic signal analyzer was used to analyze and to display the signal from the accelerometer. Experiments were conducted for the six specimens listed in Table 1. The frequency of the AC coil current of the electromagnetic device was first tuned step by step with small increments from the lower limit to the upper limit for the prescribed bandwidth. At each step, the magnitude of the AC current was tuned slowly from zero up to a saturation value to observe the dynamic response of the specimen. Since the transverse vibration amplitude of the specimen was small before instability occurred, the non-linear effects resulting from the deformation of the beam and the relative displacement between the electromagnet and the magnets were effectively avoided. At the onset of instability, the frequency and amplitude were recorded. The criterion of instability was defined as rapidly increasing amplitude of transverse vibration of the beam resulting from a small increment of the AC coil current.

The AC power source used in experiment provided AC currents with frequencies ranging from 45 to 500 Hz. The reliable excitation frequency of the beam was influenced by the mounting rigidity of the coil and coil frame and the thermoelectric effects of the coil current of the electromagnetic device on the bending rigidity of the beam. Reliable experimental results were obtained within the frequency bandwidth from 45 to about 200 Hz and the coil current up to 2 A. The specimens examined were divided into two groups in this excitation

TABLE 1

Detailed dimensions and properties of the specimens



Specimen no.	Material of beam	Length L (mm)	Width b (mm)	Thickness t (mm)	Mass of beam M (g)	Center of coil a (mm)	Mass of coil and coil frame m_0 (g)	Mass ratio of m_0/M (%)	Dimension of coil $w \times d \times h$ (mm \times mm \times mm)	No. of loops of coil	Gap between magnets g (mm)
CF1	Aluminum	200	30	1.59	26.25	17	3.09	11.8	$30 \times 30 \times 5$	30	12
CF2	Aluminum alloy	375	30.5	4.5	143.33	17	4.00	2.79	$30 \times 30 \times 8$		
CF3	Aluminum alloy	375	30.5	4.5	143.33	100	3.98	2.78	$30 \times 30 \times 8$		
CF4	Aluminum	400	30	1.59	52.50	17	3.09	5.89	$30 \times 30 \times 5$		
CF5	Aluminum alloy	600	30	3.2	157.08	17	3.97	2.53	$30 \times 30 \times 6.5$		
CF6	Aluminum alloy	600	30	3.2	158.46	230	4.02	2.54	$30 \times 30 \times 6.5$		

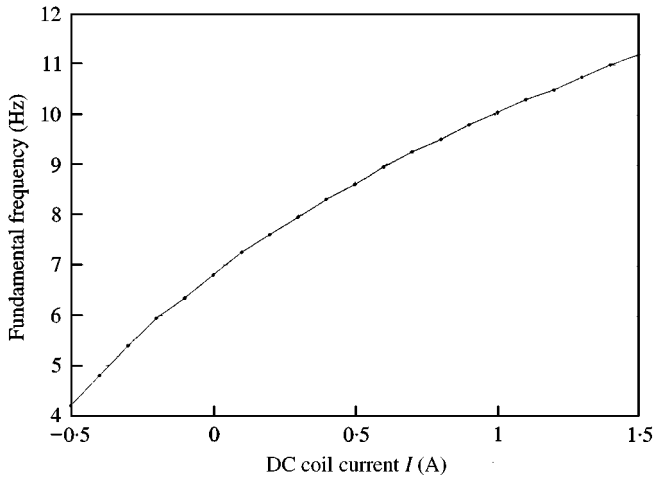


Figure 5. Relationship between fundamental natural frequency and DC coil current for specimen CF5.

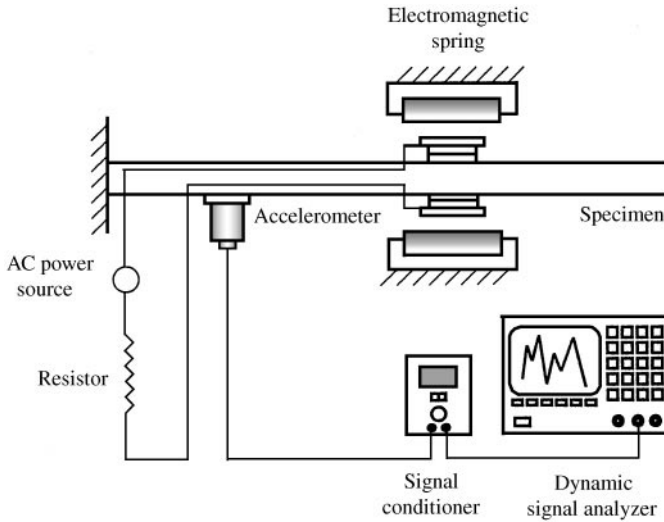


Figure 6. Experimental set-up to observe the instability behavior of specimen.

frequency range. The experiments for the first group of specimens, CF1–CF3, were performed to observe the simple resonances near twice the fundamental frequency, $2\omega_1$. For the second group of specimens, CF4–CF6, the simple resonances near twice the secondary natural frequency near $2\omega_2$, and the combination resonances, $(\omega_1 + \omega_2)$ and $(\omega_1 + \omega_3)$, were observed.

3. DYNAMIC INSTABILITY OF A BEAM UNDER TRANSVERSE EXCITATION

The beam with an electromagnetic device, shown in Figure 1, was modelled as a beam carrying a concentrated mass m_0 and a time-varying stiffness spring $k(t)$ at point P , as

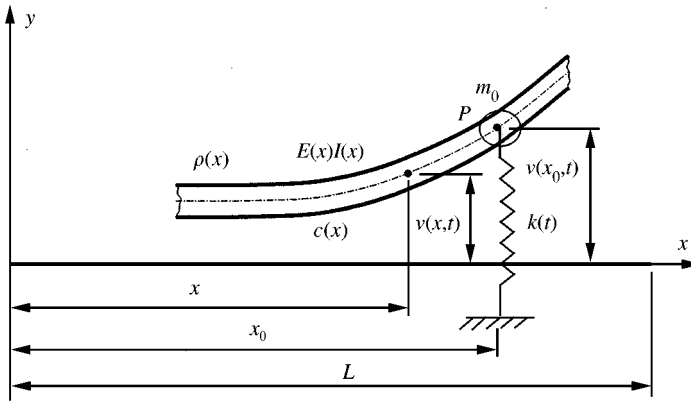


Figure 7. Dynamic system of a beam with an alternating stiffness spring in transverse direction.

shown in Figure 7. The beam has length L , mass M , mass per unit length $\rho(x)$, viscous damping coefficient $c(x)$, and bending rigidity $E(x)I(x)$. The neutral axis of the beam is initially straight. The transverse deflection of the beam is denoted by $v(x, t)$. In this work, the beam was assumed to be a Bernoulli–Euler’s beam with a small deflection in the y direction and small proportional viscous damping. The gravitational effects were neglected. When the spring $k(t)$ is removed, the partial differential equation of the system, shown in Figure 7, can be expressed as

$$[\rho(x) + m_0\delta(x - x_0)] \frac{\partial^2 v(x, t)}{\partial t^2} + c(x) \frac{\partial v(x, t)}{\partial t} + \frac{\partial^2}{\partial x^2} \left[E(x)I(x) \frac{\partial^2 v(x, t)}{\partial x^2} \right] = 0, \quad (1)$$

where $\delta(x - x_0)$ is a unit impulse function, and x_0 is the x -co-ordinate of point P . Using the assumed modes method [27], the transverse deflection of the beam $v(x, t)$ can be expressed as

$$v(x, t) = \sum_{n=1}^{\infty} \phi_n(x) V_n(t), \quad (2)$$

where $V(t)$ is a function of time and $\phi_n(x)$ is the orthonormal mode shape function which satisfies

$$\int_0^L [\rho(x) + m_0\delta(x - x_0)] \phi_n(x) \phi_m(x) dx = \delta_{nm}. \quad (3)$$

The governing equation of the free transverse vibration of the beam with a spring $k(t)$ becomes

$$\ddot{V}_n(t) + d_n \dot{V}_n(t) + \omega_n^2 V_n(t) + k(t) \sum_m \phi_n(x_0) \phi_m(x_0) V_m(t) = 0, \quad (4)$$

where d_n is the modal damping coefficient and ω_n is the undamped natural frequency. With the non-dimensionalization notations

$$\begin{aligned} \xi = x/L, \quad \tau = \omega_1 t, \quad \mu_n = d_n/2\omega_1, \quad \bar{\omega}_n = \omega_n/\omega_1, \quad \varepsilon(\tau) = k(t)/2M\omega_1^2, \\ f_{nm} = M\phi_n(x_0) \phi_m(x_0) = M\phi_n(\xi_0) \phi_m(\xi_0). \end{aligned} \quad (5)$$

One can rewrite equation (4) in the following non-dimensionalization form:

$$\ddot{V}_n(\tau) + 2\mu_n \dot{V}_n(\tau) + \bar{\omega}_n^2 V_n(\tau) + 2\varepsilon(\tau) \sum_m f_{nm} V_m(\tau) = 0, \tag{6}$$

which is the dynamic equation of the beam with a concentrated mass and a time-varying spring as shown in Figure 7.

For a system which has constant properties $\rho(x) = \rho$, $c(x) = c$, $E(x)I(x) = EI$, the governing equation of such system contains additionally off-diagonal viscous damping terms. However, when $m_0 \ll M$, the diagonal viscous damping terms are dominant and the small off-diagonal viscous damping terms can be neglected approximately. Under these conditions, the assumption of proportional damping holds and equation (6) is still valid and the damping coefficients μ_n ($n = 2, 3, 4, \dots$) can be expressed as functions of μ_1 .

When the spring has constant stiffness, $\varepsilon(\tau) = \varepsilon \neq 0$, the natural frequencies of the beam shift from $\bar{\omega}_n$ to $\hat{\omega}_n$. This variation of the natural frequencies was used to identify the spring stiffness ε in experiment. When the spring has alternating stiffness, $\varepsilon(\tau) = \varepsilon \cos \bar{\omega}\tau$, equation (6) can be rewritten as

$$\ddot{V}_n(\tau) + 2\mu_n \dot{V}_n(\tau) + \bar{\omega}_n^2 V_n(\tau) + 2\varepsilon \cos \bar{\omega}\tau \sum_m f_{nm} V_m(\tau) = 0, \quad n = 1, 2, \dots \tag{7}$$

Equation (7) is a Mathieu's equation with parametrically excited terms associated with modal displacements V_n . This equation was used to express the dynamic behavior of the beam subjected to the parametric excitation caused by the alternating stiffness spring. The parametric excitation coefficients f_{nm} in equation (7) are functions of the mode shapes ϕ_n and of the mass of the beam M . Once the coefficients f_{nm} are found, the instability bandwidth of the simple and combination resonances of Mathieu's equation (7) can be determined using the amplitude of the spring stiffness ε , the natural frequencies of the beam $\bar{\omega}_n$, $\bar{\omega}_m$, and the instability bandwidth parameters G_{nm} [21] as follows:

(1) *Simple resonance*. When the excitation frequency $\bar{\omega}$ is close to $2\bar{\omega}_n$ and the instability bandwidth parameter G_{nn} defined as

$$G_{nn} = \begin{cases} (f_{nn}/\bar{\omega}_n)^2 - 4(\mu_n/\varepsilon)^2, & \mu_n \neq 0, \\ (f_{nn}/\bar{\omega}_n)^2, & \mu_n = 0, \end{cases} \tag{8}$$

the transition curves separating stable and unstable regions are

$$\bar{\omega} = 2\bar{\omega}_n \pm \varepsilon G_{nn}^{1/2} \quad \text{for } G_{nn} > 0. \tag{9}$$

(2) *Combination resonance of sum type*. When the excitation frequency $\bar{\omega}$ is near $\bar{\omega}_n + \bar{\omega}_m$ and the instability bandwidth parameter G_{nm} defined as

$$G_{nm} = \begin{cases} (\mu_n + \mu_m)^2 [f_{nm} f_{mn} / 4\bar{\omega}_n \bar{\omega}_m - \mu_n \mu_m / \varepsilon^2] / \mu_n \mu_m, & \mu_n \text{ or } \mu_m \neq 0, \\ f_{nm} f_{mn} / 4\bar{\omega}_n \bar{\omega}_m, & \mu_n, \mu_m = 0, \end{cases} \tag{10}$$

the transition curves separating stable and unstable regions are

$$\bar{\omega} = \bar{\omega}_n + \bar{\omega}_m \pm \varepsilon G_{nm}^{1/2} \quad \text{for } G_{nm} > 0. \tag{11}$$

(3) *Combination resonance of difference type*. When the excitation frequency $\bar{\omega}$ is near $\bar{\omega}_n - \bar{\omega}_m$, $\bar{\omega}_n > \bar{\omega}_m$ and the instability bandwidth parameter G_{nm} defined as

$$G_{nm} = \begin{cases} (\mu_n + \mu_m)^2 [-f_{nm} f_{mn} / 4\bar{\omega}_n \bar{\omega}_m - \mu_n \mu_m / \varepsilon^2] / \mu_n \mu_m, & \mu_n \text{ or } \mu_m \neq 0, \\ -f_{nm} f_{mn} / 4\bar{\omega}_n \bar{\omega}_m, & \mu_n, \mu_m = 0, \end{cases} \tag{12}$$

the transition curves separating stable and unstable regions are

$$\bar{\omega} = \bar{\omega}_n - \bar{\omega}_m \pm \varepsilon G_{nm}^{1/2} \quad \text{for } G_{nm} > 0. \tag{13}$$

For the dynamic system considered in Figure 7, all the parametric excitation coefficients f_{nm} in equation (7) are of symmetric form. Therefore, the combination resonance of difference type does not occur. Moreover, the critical excitation amplitude is defined as [11]

$$\varepsilon_{cr} = (\mu_n \mu_m / G_{nm})^{1/2}, \tag{14}$$

which is a minimum value of excitation amplitude, below which the system is always stable. The viscous damping ratios of the system can be identified from ε_{cr} .

4. RESULTS AND DISCUSSION

Figure 8 shows the relationship between the non-dimensionalized spring stiffness ε and the DC coil current I of the electromagnetic device for specimen CF1. The non-dimensionalized spring stiffness ε is defined in equation (5) as $\varepsilon = k/2M\omega_1^2$. The data points were obtained using equation (6) to analytically tune the spring stiffness ε for the same measured transverse fundamental frequency as a DC current flowing through the coil of the electromagnetic device. Figure 8 shows that the spring stiffness ε and the DC coil current I have a good linear correlation. The proportionality between the spring stiffness ε and the DC coil current I was found by the curve-fitting technique. The ratios ε/I of specimens CF2–CF6 also possess good linearity as that of CF1. The ratios between the spring stiffness ε and the DC coil current I of all specimens and the first three natural frequencies of the specimens without an electromagnetic device (zero DC coil current) are presented in Table 2.

Physically, the ratio between the spring constant k and the coil current I of the electromagnetic device depends on the gap between the two magnets, the beam thickness, the dimension and loop numbers of the coil, and the relative position of the coil to the magnets. In experiments, the gap of magnets and the loop numbers of the coil were kept constant; thus, the ratio k/I remained almost the same when the thickness of the beam was constant. However, as defined in equation (5), the non-dimensionalized spring stiffness ε is

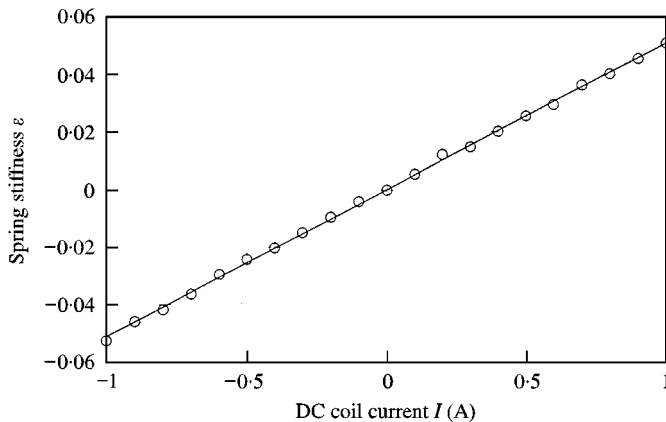


Figure 8. Relationship between spring stiffness and DC coil current for specimen CF1.

TABLE 2
Modal parameters of the specimens

Specimen no.	Non-dimensionalized theoretical natural frequencies of specimens			Experimental natural frequencies of specimens (Hz)			Non-dimensionalized experimental natural frequencies of specimens (Hz)			Theoretical ratios of modal damping coefficients		Ratio ε/I	Experimental modal damping coefficient μ_1 (from critical excitation amplitude ε_{cr} of various resonance modes)			
	$\bar{\omega}_1$	$\bar{\omega}_2$	$\bar{\omega}_3$	ω_1	ω_2	ω_3	$\bar{\omega}_1$	$\bar{\omega}_2$	$\bar{\omega}_3$	μ_2/μ_1	μ_3/μ_1		$2\omega_1$	$\omega_1 + \omega_2$	$2\omega_2$	$\omega_1 + \omega_3$
CF1	1	6.922	20.17	27.875	187.5	554	1	6.726	19.87	1.1436	1.2238	0.0990	0.0045			
CF2	1	6.372	18.04	24.875	158.25	447	1	6.362	17.97	1.0255	1.0445	0.0233	0.012			
CF3	1	6.394	17.58	25.50	163.0	450	1	6.392	17.65	1.0351	1.0019	0.0235	0.0076			
CF4	1	6.500	18.59	7.375	48.0	135.5	1	6.508	18.37	1.0428	1.0752	0.6953		0.012	0.012	0.011
CF5	1	6.338	17.89	6.875	43.625	123.0	1	6.345	17.89	1.0412	1.0257	0.2505		0.015	0.014	0.019
CF6	1	6.246	17.52	7.20	45.25	126.5	1	6.285	17.57	0.9935	0.9955	0.2334		0.008	0.012	0.011

equal to $k/2M\omega_1^2$ and the ratio ε/I is inversely proportional to the value $(M\omega_1^2)$ of the beam with constant thickness. From Tables 1 and 2, beam specimens CF2 and CF3 have the same thickness and the close corresponding $(M\omega_1^2)$ values; therefore, the ratios ε/I of CF2 and CF3 are almost the same. Similarly, the ratio ε/I of CF5 and CF6 are roughly the same, too. However, the $(M\omega_1^2)$ ratio between CF1 and CF4, $(M\omega_1^2)_{CF1}/(M\omega_1^2)_{CF4}$, is roughly equal to 7, thus the corresponding ratio $(\varepsilon/I)_{CF1}/(\varepsilon/I)_{CF4}$ is almost equal to 1/7.

It is noted that the electromagnetic device possesses either positive or negative stiffness, and the spring stiffness can be adjusted by the current flowing through the coil. As the electromagnetic device is connected to a structure, it can add or remove stiffness from that structure. In other words, the electromagnetic device can be employed to regulate the natural frequency of a structure. This property is useful in the vibration suppression of structures.

According to the available frequency range in experimental set-up, the instability behavior of the specimens CF1–CF3 was observed on the transition curves of the simple resonance near twice of the fundamental frequency, $2\bar{\omega}_1$. The instability behavior of specimens CF4–CF6 was observed on the transition curves of the simple resonance near twice of the secondary natural frequency, $2\bar{\omega}_2$, and the combination resonance near $(\bar{\omega}_1 + \bar{\omega}_2)$ and $(\bar{\omega}_1 + \bar{\omega}_3)$. The analytical results of the transition curves of the simple and combination resonances of the six specimens with various viscous damping coefficients are also presented. As mentioned in the previous section, the modal damping coefficients μ_n can be expressed as functions of μ_1 . The theoretical ratios of μ_2/μ_1 and μ_3/μ_1 are given in Table 2.

Figures 9–14 show the instability regions of the specimens CF1–CF6 respectively. The analytical results of the transition curves of the simple and the combination resonances with various viscous modal damping coefficients μ_n are shown with the experimental results. The

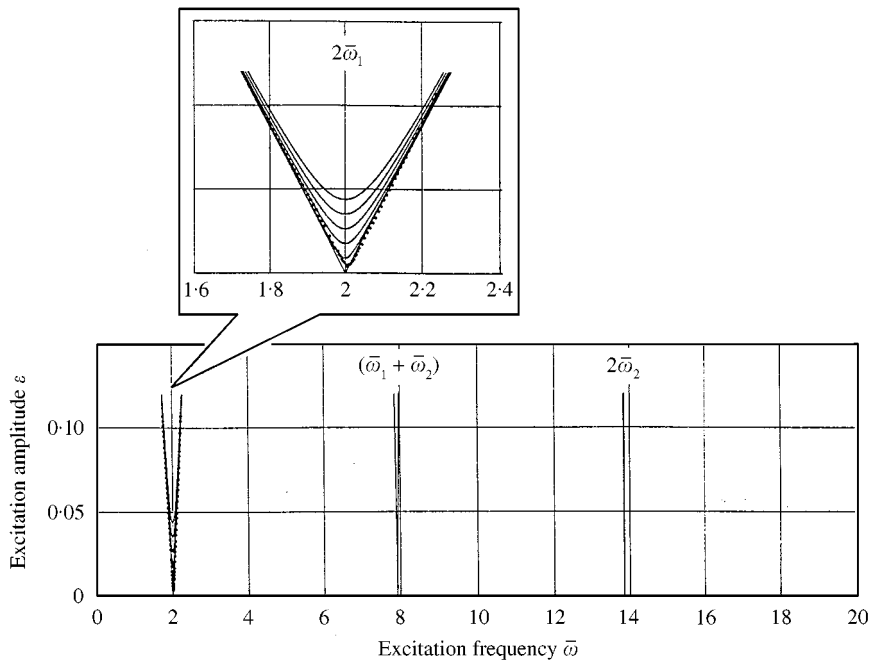


Figure 9. Instability regions of specimen CF1: —, analytical results (from bottom up $\mu_1 = 0, 0.01, 0.02, 0.03, 0.04$ and 0.05); ·····, experimental data.

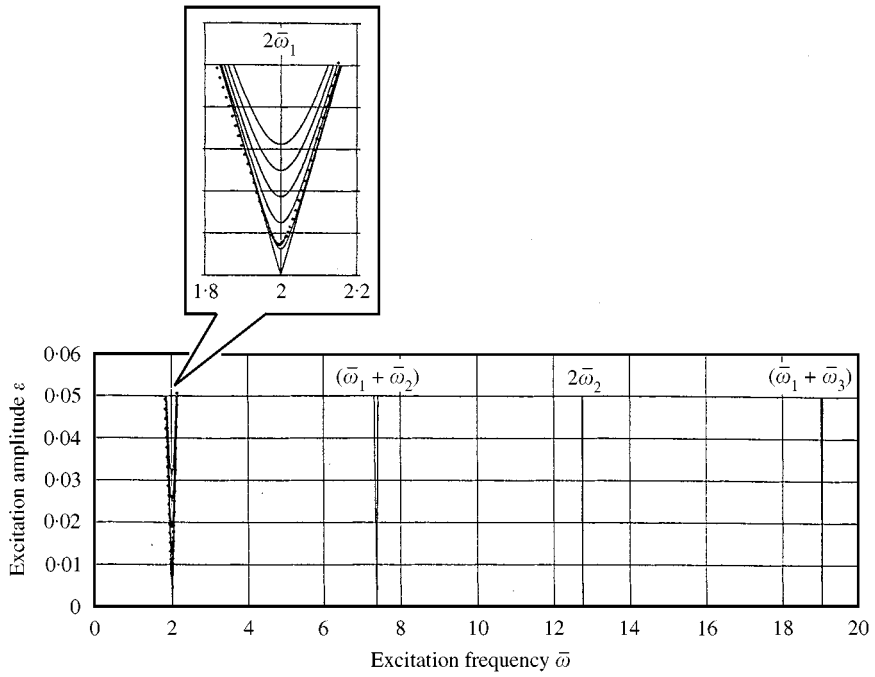


Figure 10. Instability regions of specimen CF2: —, analytical results (from bottom up $\mu_1 = 0, 0.01, 0.02, 0.03, 0.04$ and 0.05); \cdots , experimental data.

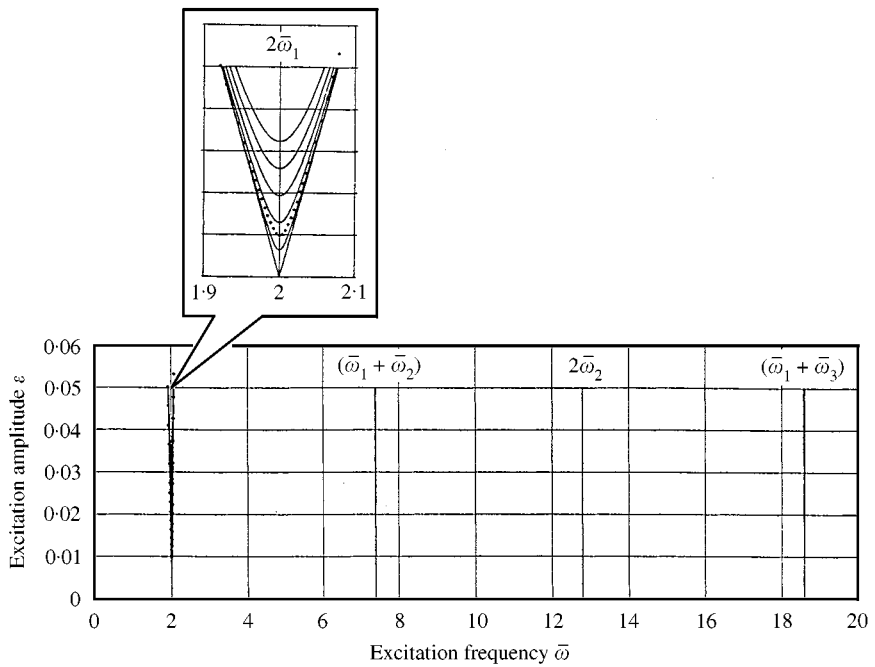


Figure 11. Instability regions of specimen CF3: —, analytical results (from bottom up $\mu_1 = 0, 0.005, 0.01, 0.015, 0.02$ and 0.025); \cdots , experimental data.

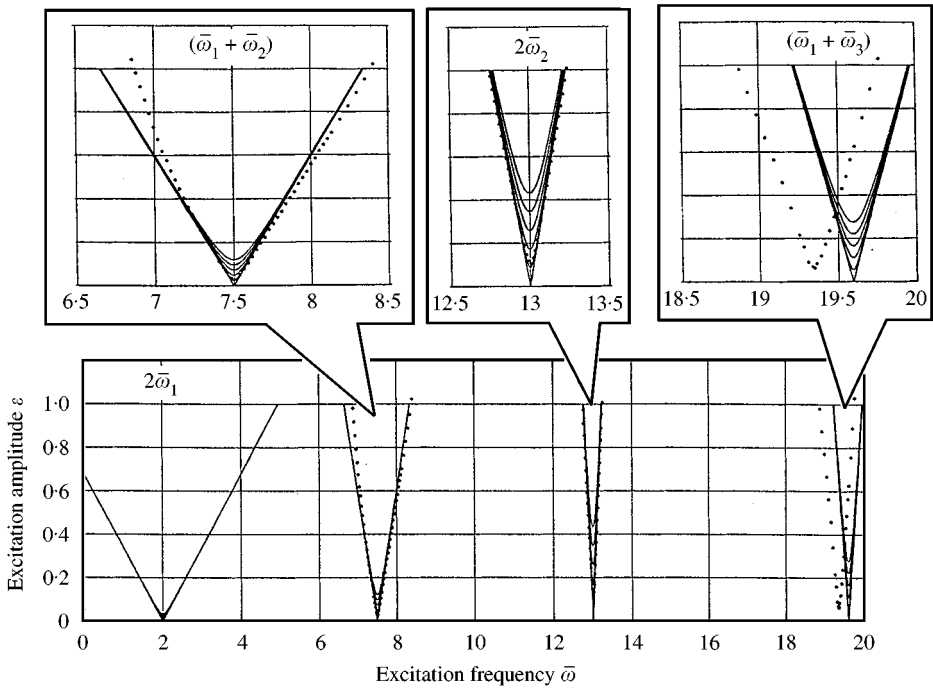
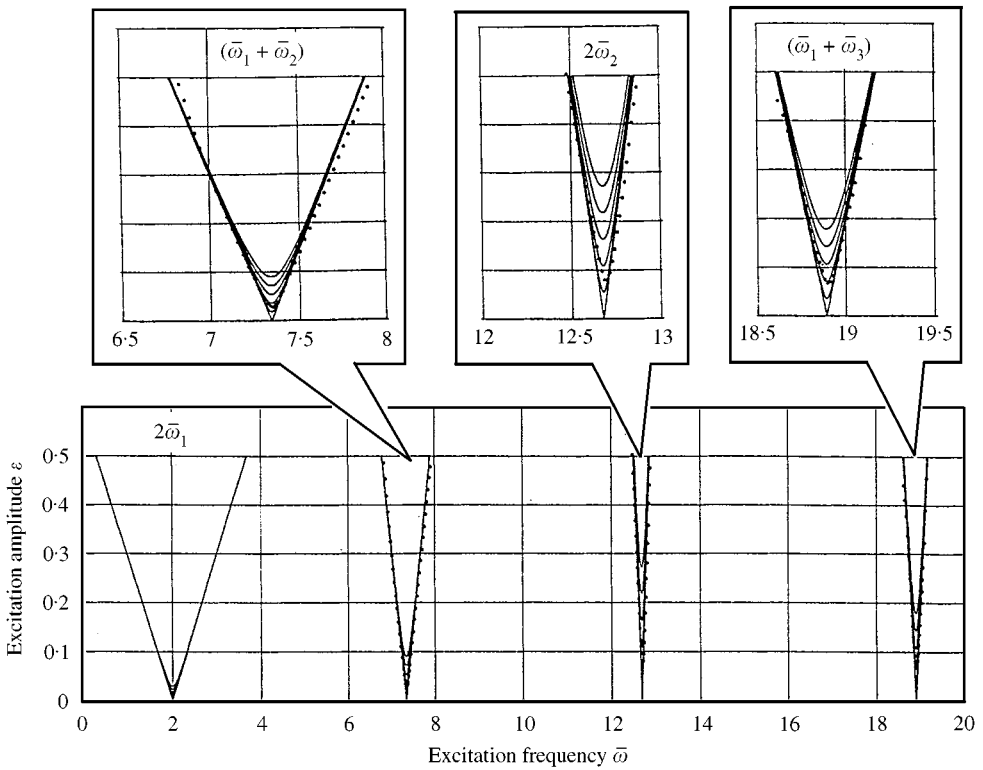


Figure 12. Instability regions of specimen CF4: —, analytical results (from bottom up $\mu_1 = 0, 0.01, 0.02, 0.03, 0.04$ and 0.05); \cdots , experimental data.



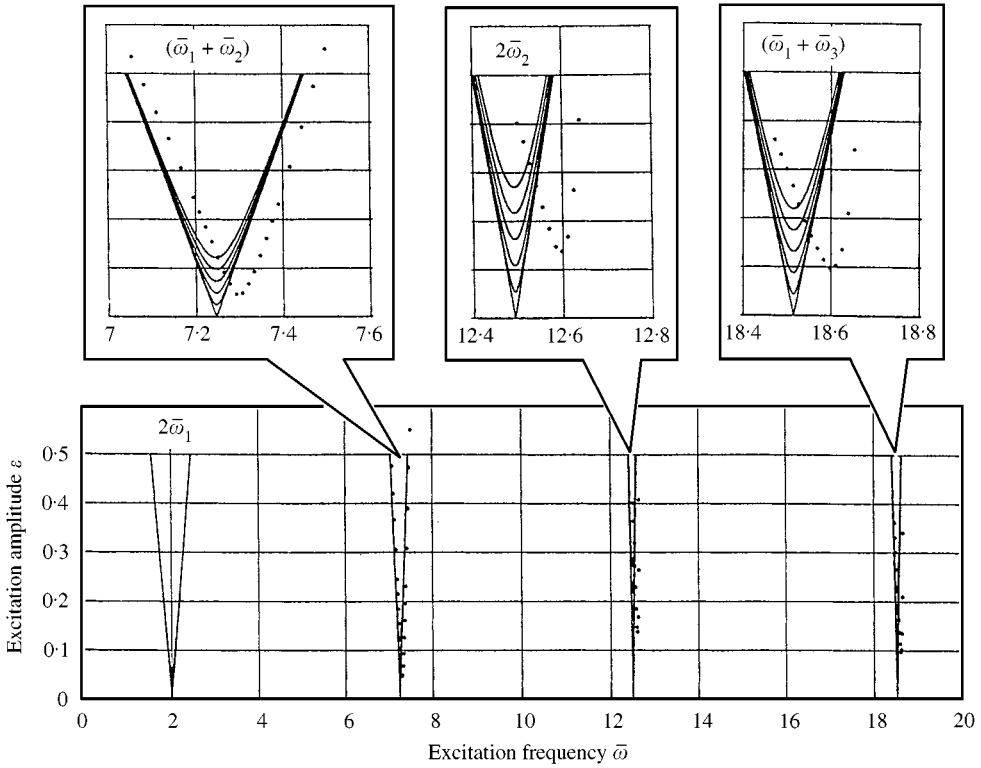


Figure 14. Instability regions of specimen CF6. — analytical results (from bottom up $\mu_1 = 0, 0.005, 0.01, 0.015, 0.02$ and 0.025); \dots experimental data.

cases with experimental points on the transition curves are also magnified in Figures 9–14. In Figures 9–14, the experimental results and the analytical ones are in good agreement which results from the non-contacting nature of the electromagnetic device acting transversely on the beam in experiments. Moreover, using equation (14), the modal damping coefficient μ_1 of CF1–CF6 can be identified and the results are given in Table 2. The disturbances, occurring usually in “periodically axial loading” or “periodically axial motion”, induced by the geometric imperfection of the beam, the eccentric effects of the axial excitation force and the coupling effects between the specimen and the excitation mechanism, can be effectively avoided.

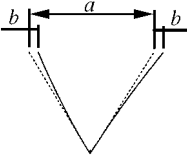
Moreover, the amplitude of the excitation current was limited to 2 A to avoid overheating the coil and the non-linearity of the transition curve resulting from high loading amplitude was neglected. Table 3 shows the deviation of the present instability bandwidth at various resonant frequencies when compared with the instability bandwidth including the second order term derived by Nayfeh and Mook [3] at specified excitation amplitude. The results obtained from the first order expansion are much simpler than those including the second order term. In Table 3, larger deviations occurred for specimen CF4, which was under larger specified excitation amplitude. For example, the instability bandwidth of the first order expansion of CF4 shifted 7.6% to the left when compared with

Figure 13. Instability regions of specimen CF5: —, analytical results (from bottom up $\mu_1 = 0, 0.01, 0.02, 0.03, 0.04$ and 0.05); \dots , experimental data.

TABLE 3

Deviation of instability bandwidth between the first and second order expansion at specified excitation amplitude

Specimen no.	Max. excitation amplitude ε_{max}	$b/a \times 100\%$			
		$2\omega_1$ (%)	$2\omega_2$ (%)	$\omega_1 + \omega_2$ (%)	$\omega_1 + \omega_3$ (%)
CF1	0.11	- 1.8	0.33	0.94	0.58
CF2	0.05	- 1.3	0.27	0.38	0.23
CF3	0.05	- 0.53	0.15	0.48	0.03
CF4	1.0	- 23	4.8	7.6	4.3
CF5	0.5	- 14	3.0	3.3	2.1
CF6	0.5	4.7	1.0	0.28	0.46



--- First order expansion (present)
 $\bar{\omega} = \bar{\omega}_n + \bar{\omega}_m \pm \varepsilon G_{nm}^{1/2}$
 — Second order expansion [3]

$$\bar{\omega} = \bar{\omega}_n + \bar{\omega}_m \pm \varepsilon G_{nm}^{1/2} - 0.5\varepsilon^2 \left\{ 0.25G_{nm}(\bar{\omega}_n^{-1} + \bar{\omega}_m^{-1}) - \sum_r \bar{\omega}_r \left[\frac{G_{nm}}{(\bar{\omega}_n + 2\bar{\omega}_m)^2 - \bar{\omega}_r^2} - \frac{G_m}{(2\bar{\omega}_n + \bar{\omega}_m)^2 - \bar{\omega}_r^2} \right] - \sum_{r \neq n} \frac{\bar{\omega}_r G_{nm}}{\bar{\omega}_n^2 - \bar{\omega}_r^2} - \sum_{r \neq m} \frac{\bar{\omega}_r G_m}{\bar{\omega}_m^2 - \bar{\omega}_r^2} \right\}$$

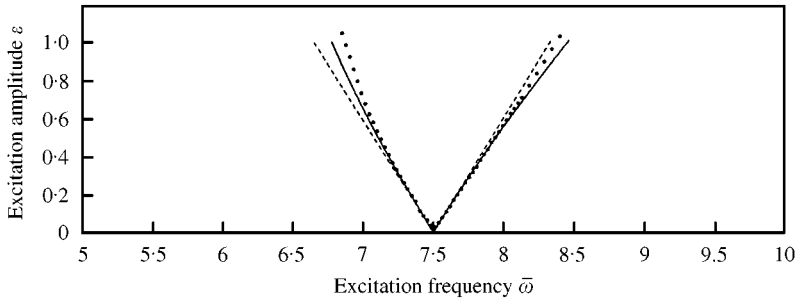


Figure 15. Transition curves of specimen CF4 at frequency $(\bar{\omega}_1 + \bar{\omega}_2)$. --- first order expansion; — second order expansion; ···· experimental data.

that of the second order expansion for the combination resonance near $(\bar{\omega}_1 + \bar{\omega}_2)$ at excitation amplitude $\varepsilon = 1.0$. Figure 15 shows the transition curves of this case together with the experimental data of specimen CF4. Although the results including the second order term are closer to the experimental ones, the results of the first order expansion also agree well, especially for the cases with smaller excitation amplitude.

5. CONCLUSIONS

An electromagnetic device, acting like an alternating stiffness spring, was developed to examine the parametric instability regions of a beam. The experimental results are found to

agree well with the analytical ones. The viscous modal damping coefficients of the specimens can be identified from the experimental results. This technique is a potentially good tool in the experimental investigation of parametric instability behavior of various structures with various materials. Additionally, it is noted that:

- (1) While observing the instability of the specimen, the AC coil current was always tuned from zero up to the magnitude at the onset of instability. The transverse vibration of the specimen was easily controlled in small amplitude before the instability occurred; therefore, the non-linear effects resulting from the deformation of the specimen and the relative displacement between the coil and the magnets of the electromagnetic device were effectively avoided.
- (2) Since the non-contacting electromagnetic device possesses either the positive or negative stiffness, it can be employed to add or to remove stiffness from a structure without changing the structure. This property is useful in the vibration suppression of structures.

REFERENCES

1. V. V. BOLOTIN 1965 *The Dynamic Stability of Elastic Systems*. New York: Holden-Day Inc.
2. R. M. EVAN-IWANOWSKI 1965 *Applied Mechanics Review* **18**, 699–702. On the parametric response of structures.
3. A. H. NAYFEH and D. T. MOOK 1979 *Nonlinear Oscillations*. New York: Wiley Inc.
4. C. S. HSU 1961 *Journal of Applied Mechanics* **28**, 551–556. On a restricted class of coupled Hill's equations and some applications.
5. C. S. HSU 1963 *Journal of Applied Mechanics* **30**, 367–372. On the parametric excitation of a dynamic system having multiple degrees of freedom.
6. C. S. HSU 1965 *Journal of Applied Mechanics* **32**, 373–377. Further results on parametric excitation of a dynamic system.
7. A. H. NAYFEH and D. T. MOOK 1977 *Journal of Acoustical Society of America* **62**, 375–381. Parametric excitations of linear systems having many degrees of freedom.
8. C. H. J. FOX 1990 *Journal of Sound and Vibration* **136**, 275–287. Parametrically excited instability in a lightly damped multi-degree-of-freedom system with gyroscopic coupling.
9. T. IWATSUBO, Y. SUGIYAMA and K. ISHIHARA 1972 *Journal of Sound and Vibration* **23**, 245–257. Stability and non-stationary vibration of columns under periodic loads.
10. T. IWATSUBO, M. SAIGO and Y. SUGIYAMA 1973 *Journal of Sound and Vibration* **30**, 65–77. Parametric instability of clamped-clamped and clamped-simply supported columns under periodic axial load.
11. T. IWATSUBO, Y. SUGIYAMA and OGINO 1974 *Journal of Sound and Vibration* **33**, 211–221. Simple and combination resonances of columns under periodic axial loads.
12. H. A. EVENSEN and R. M. EVAN-IWANOWSKI 1966 *Journal of Applied Mechanics* **33**, 141–148. Effects of longitudinal inertia upon the parametric response of elastic columns.
13. K. SATO, H. SAITO and K. OTOMI 1978 *Journal of Applied Mechanics* **45**, 643–648. The parametric response of a horizontal beam carrying a concentrated mass under gravity.
14. M. Y. YEH and C. C. CHEN 1998 *Journal of Sound and Vibration* **217**, 665–689. Dynamic instability of a general column under periodic load in the direction of the tangency coefficient at any axial position.
15. K. L. HANDOO and V. SUNDARARAJAN 1971 *Journal of Sound and Vibration* **18**, 45–53. Parametric instability of a cantilevered column with end mass.
16. R. ELMARAGHY and B. TABARROK 1975 *Journal of the Franklin Institute* **300**, 25–39. On the dynamic stability of an axially oscillating beam.
17. H. SAITO and N. KOIZUMI 1982 *International Journal of Mechanical Sciences* **24**, 755–761. Parametric vibrations of a horizontal beam with a concentrated mass at one end.
18. M. GURGOZE 1986 *Journal of Sound and Vibration* **108**, 73–84. Parametric vibrations of a restrained beam with an end mass under displacement excitation.
19. K. W. BUFFINTON and T. R. KANE 1985 *International Journal of Solids and Structures* **21**, 617–643. Dynamics of a beam moving over supports.

20. M. GURGOZE 1985 *Journal of Sound and Vibration* **102**, 415–422. On the dynamic stability of a pre-twisted beam subject to a pulsating axial load.
21. C. C. CHEN and M. K. YEH 1999 *Journal of Sound and Vibration* **224**, 643–664. Parametric instability of a column with an axially oscillating mass.
22. K. K. STEVENS and R. M. EVAN-IWANOWSKI 1969 *International Journal of Solids and Structures* **5**, 755–765. Parametric resonance of viscoelastic columns.
23. G. CEDERBAUM and M. MOND 1992 *Journal of Applied Mechanics* **59**, 16–19. Stability properties of a viscoelastic column under a periodic force.
24. M. GURGOZE 1987 *Journal of Sound and Vibration* **115**, 329–338. Parametric vibrations of a viscoelastic beam (Maxwell model) under steady axial load and transverse displacement excitation at one end.
25. K. RAY and R. C. KAR 1996 *Journal of Sound and Vibration* **193**, 631–644. Parametric instability of multi-layered sandwich beams.
26. K. RAY and R. C. KAR 1996 *Journal of Sound and Vibration* **197**, 137–152. The parametric instability of partially covered sandwich beams.
27. R. R. CRAIG JR 1981 *Structural Dynamics*. New York: John Wiley.